Arch Appl Mech (2017) 87:365–384
DOI 10.1007/s00419-016-1198-5

ORIGINAL

P. Geng · J. Z. Xing · X. X. Chen

Winding angle optimization of filament-wound cylindrical vessel under internal pressure

Received: 11 April 2016 / Accepted: 18 October 2016 / Published online: 1 November 2016

Abstract The maximum strength ratio and more uniform strength for all layers can be achieved by variation of winding angle of filament-wound (FW) vessel. The deformation and stresses of a thick-walled cylinder with multi-angle winding filament under uniform internal pressure are proposed. The stresses of each orthotropic unit of fiber layers, as well as longitudinal stress along the fiber direction, transverse stresses perpendicular to the fiber direction and shear stress in the fiber layer are derived analytically. An optimization model of FW closed ends vessel under uniform internal pressure subjected to Tsai–Wu failure criterion to maximize the lowest strength ratio through thickness with optimal variation of winding angle is built. Two optimization methods are adopted to find the optimized winding angle sequence through different ways, and their combination led to more efficient algorithm is suggested. The research shows that the material utilization and working pressure can be increased by proper winding angle variation, and several optimization winding angle sequence schemes are found for different thickness ratios cylindrical vessels with two typical composite materials E-glass/epoxy and T300/934, which are useful for many applications of FW vessel design and manufacture.

Keywords Multi-layered · Complex method · Steepest descent · Glass fibers · Carbon fibers · Fiber stress

1 Introduction

With the development of science and technology, high-performance fiber-wound pressure vessel has been widely used in many fields, such as rocket, missile, deep diving, satellite [1]. And the mechanical performances of winding filaments differ in thousands ways. Filament-wound (FW) structure can remedy the shortcomings and take the advantages. Modern computerized equipment allows for the production of multi-angle winding structures [2]. However, how to design a FW structure with proper winding angle to maximize the material utilization is still a challenged task today.

Using internal pressure and axial force, experiments under biaxial tensile stress ratios were carried out to investigate the performance of multi-angle FW structures [3]. Multi-angle wound structures exhibit better performance in resisting damage and greater advantages over pure angle-ply lay-ups [4]. Many experimental

P. Geng (✉)
School of Aeronautic Science and Engineering, Beihang University, Beijing 100191, China
E-mail: gp321.cool@163.com

J. Z. Xing
School of Mechanical Engineering, Tianjin Polytechnic University, Tianjin 300387, China
E-mail: hsingjzh@tjpu.edu.cn

X. X. Chen
Tianjin Key Laboratory of Advanced Mechatronics Equipment Technology, Tianjin 300387, China
E-mail: chenxx@tjpu.edu.cn

failure analyses [5–9] have been conducted for pipes with different winding angles, and an optimum winding angle of 55° has been noted for thin pipes subjected to internal pressure or biaxial loads with a hoop-to-axial stress ratio of 2:1. Researches show that stacking sequence has great influence on pressure capability [10,11], where stacking sequence can only be computed by 3-D analysis [12]. Using 3-D orthotropic elasticity and axisymmetric thick-walled cylinder theory, deformation and stresses of a thick cylinder using multi-angle winding with different kinds of filaments with any number of layers under internal, external pressure and axial force are investigated analytically [13].

Base on 3-D anisotropic elasticity, many optimization researches of composite structure have been proposed. However, part of the optimization researches focused on minimizing the weight and thickness of composite laminates with different methods [14–17]. After that, an integrated optimization methodology is proposed to optimize the manufacturing cost as well as the structural performance of composite laminated plates manufactured by the resin transfer molding (RTM) process [18]. A new initialization strategy is proposed by Irisarri et al. following mechanical considerations. The method is applied to the optimal design of a composite plate for weight minimization and maximization of the buckling margins under three hundred load cases that make also the originality of this work [19]. A technique for the optimization design of composite laminated structures is presented, and the optimization process is performed using a genetic algorithm (GA), associated with the finite element method for the structural analysis [20]. The layer optimization was carried out for maximum fundamental frequency of laminated composite plates under any combination of three classical edge conditions [21]. A new iteration fractal branch and bound method is proposed, which does not require empirical knowledge of the target structure [22]. Gre'diac dealt with the stiffness design of laminated plates made of woven plies [23]. All the above researches are concerned about composite laminates. The optimization of FW thick-walled cylindrical vessel with variation of winding angle has been investigated early in 1988 [1]. Until 2006, an optimization of multilayered composite pressure vessels is accomplished using GA and subject to the Tsai–Wu failure criterion [24], but the optimal variation of winding angle is still undetermined for commonly used composite material.

Here, the deformation and stresses of a thick-walled cylinder using multi-angle winding with different kinds of filament with any number of layers under uniform internal pressure are investigated analytically. To be convenient for strength assessment, longitudinal stress along fiber direction, transverse stresses perpendicular to the fiber direction and shear stress are present analytically. An optimization model of multiple winding angle FW cylindrical vessel under uniform pressure is built, to maximize the lowest strength ratio in all layers by adjusting the winding angle of each layer. Two traditional optimization methods are adopted to find the optimization results, and their calculation efficiency is compared. Numeric results show that their combination has better efficiency to achieve the optimization solution.

2 Stresses in fiber layer

Consider a thick-walled cylinder with an inner radius of r_0, and outer radius after alternate-ply FW of r_n. Each alternate-ply layer can be regarded as an orthotropic layer. Winding filaments are divided into n orthotropic layers with outer radius of r_i, $(i = 1, 2, \ldots, n)$, with different kinds of filament and winding angles in each layer.

The cylinder is subjected to uniform internal pressure q_a. Only displacement in radial r direction and axial z direction occurs, and axisymmetric stresses are developed for all orthotropic layers (Fig. 1).

2.1 On-axis stress–strain relation

The ply-oriented constitutive relationship can be expressed in matrix form as

$$\{\sigma\} = \begin{Bmatrix} \sigma_1 \\ \sigma_2 \\ \sigma_3 \\ \tau_{23} \\ \tau_{31} \\ \tau_{12} \end{Bmatrix} = \begin{bmatrix} C_{11} & C_{12} & C_{13} & 0 & 0 & 0 \\ C_{12} & C_{22} & C_{23} & 0 & 0 & 0 \\ C_{13} & C_{23} & C_{33} & 0 & 0 & 0 \\ 0 & 0 & 0 & G_{23} & 0 & 0 \\ 0 & 0 & 0 & 0 & G_{31} & 0 \\ 0 & 0 & 0 & 0 & 0 & G_{12} \end{bmatrix} \begin{Bmatrix} \varepsilon_1 \\ \varepsilon_2 \\ \varepsilon_3 \\ \gamma_{23} \\ \gamma_{31} \\ \gamma_{12} \end{Bmatrix} = [C]\{\varepsilon\} \tag{1}$$

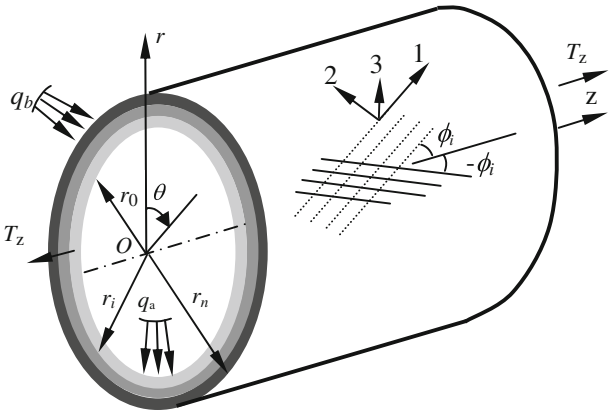

Fig. 1 Axisymmetric filament-wound cylinder

In which

$$[C] = \begin{bmatrix} 1/E_1 & -\nu_{12}/E_2 & -\nu_{13}/E_3 & 0 & 0 & 0 \\ -\nu_{21}/E_1 & 1/E_2 & -\nu_{23}/E_3 & 0 & 0 & 0 \\ -\nu_{31}/E_1 & -\nu_{32}/E_2 & 1/E_3 & 0 & 0 & 0 \\ 0 & 0 & 0 & 1/G_{23} & 0 & 0 \\ 0 & 0 & 0 & 0 & 1/G_{31} & 0 \\ 0 & 0 & 0 & 0 & 0 & 1/G_{12} \end{bmatrix}^{-1} \tag{2}$$

For unidirectional orientation fiber composites, the fiber distributions are very similar in the 2 and 3 directions. Therefore, assuming transverse isotropy, and based on equivalent properties in the 2–3 plane for unidirectional material, we have

$$\begin{aligned} &E_2 = E_3, \quad G_{31} = G_{12}, \quad \nu_{12} = \nu_{13}, \\ &\nu_{21} = \nu_{31}, \quad G_{23} = E_2/2/(1+\nu_{23}) \end{aligned} \tag{3}$$

Then, the stiffness matrix in Eq. (2) can be simplified as

$$[C]_{3\times 3} = \frac{1}{1 - \frac{2\nu_{21}^2}{1-\nu_{23}}\frac{E_2}{E_1}} \begin{bmatrix} E_1 & \frac{\nu_{21}E_2}{1-\nu_{23}} & \frac{\nu_{21}E_2}{1-\nu_{23}} \\ & \frac{1-\nu_{21}^2 E_2/E_1}{1-\nu_{23}^2}E_2 & \frac{\nu_{23}+\nu_{21}^2 E_2/E_1}{1-\nu_{23}^2}E_2 \\ \text{sym.} & & \frac{1-\nu_{21}^2 E_2/E_1}{1-\nu_{23}^2}E_2 \end{bmatrix}$$

$$C_{44} = \frac{E_2}{2(1+\nu_{23})}, \quad C_{55} = C_{66} = G_{12} \tag{4}$$

2.2 Off-axis stress–strain relation

The strain energy can be calculated with on-axis stiffness constants or off-axis stiffness constants. With coordinate transformation of the strain vector, we can get the relationship between the stiffness coefficients of on-axis and that of off-axis, which is

$$[\bar{C}] = [T_\varepsilon]^T [C][T_\varepsilon] \tag{5}$$

The nonzero elements of $\bar{C}_{ij}$, $(i, j = 1, 2, 3)$ can be expressed in matrix form as

$$\begin{Bmatrix} \bar{C}_{11} \\ \bar{C}_{22} \\ \bar{C}_{33} \\ \bar{C}_{23} \\ \bar{C}_{13} \\ \bar{C}_{12} \end{Bmatrix} = \begin{bmatrix} m^4 & n^4 & 0 & 2m^2n^2 & 0 & 0 & 4m^2n^2 \\ n^4 & m^4 & 0 & 2m^2n^2 & 0 & 0 & 4m^2n^2 \\ 0 & 0 & 1 & 0 & 0 & 0 & 0 \\ 0 & 0 & 0 & 0 & n^2 & m^2 & 0 \\ 0 & 0 & 0 & 0 & m^2 & n^2 & 0 \\ m^2n^2 & m^2n^2 & 0 & m^4+n^4 & 0 & 0 & -4m^2n^2 \end{bmatrix} \begin{Bmatrix} C_{11} \\ C_{22} \\ C_{33} \\ C_{12} \\ C_{13} \\ C_{23} \\ G_{12} \end{Bmatrix} \tag{6}$$

For a group of plies within an alternate-ply layer, the effective average properties of the layers are $\bar{C}_{ij}$, $(i, j = 1, 2, 3)$. For layer (i), the orthotropic stress–strain relationship can be written as

$$\begin{Bmatrix} \sigma_z^{(i)} \\ \sigma_\theta^{(i)} \\ \sigma_r^{(i)} \end{Bmatrix} = \begin{bmatrix} \bar{C}_{11}^{(i)} & \bar{C}_{12}^{(i)} & \bar{C}_{13}^{(i)} \\ \bar{C}_{12}^{(i)} & \bar{C}_{22}^{(i)} & \bar{C}_{23}^{(i)} \\ \bar{C}_{13}^{(i)} & \bar{C}_{23}^{(i)} & \bar{C}_{33}^{(i)} \end{bmatrix} \begin{Bmatrix} \varepsilon_z^{(i)} \\ \varepsilon_\theta^{(i)} \\ \varepsilon_r^{(i)} \end{Bmatrix} = \begin{bmatrix} \bar{C}_{zz}^{(i)} & \bar{C}_{z\theta}^{(i)} & \bar{C}_{zr}^{(i)} \\ \bar{C}_{z\theta}^{(i)} & \bar{C}_{\theta\theta}^{(i)} & \bar{C}_{\theta r}^{(i)} \\ \bar{C}_{zr}^{(i)} & \bar{C}_{\theta r}^{(i)} & \bar{C}_{rr}^{(i)} \end{bmatrix} \begin{Bmatrix} \varepsilon_z^{(i)} \\ \varepsilon_\theta^{(i)} \\ \varepsilon_r^{(i)} \end{Bmatrix} \tag{7}$$

2.3 Deformation and stresses

Considering the equilibrium equation in radial displacement, whose solution can be expressed as

$$u_r^{(i)}(r) = D_1^{(i)} r^{s_i} + D_2^{(i)} r^{-s_i} + t_1^{(i)} \varepsilon_0 r \tag{8a}$$

where

$$s_i = \sqrt{\bar{C}_{\theta\theta}^{(i)} / \bar{C}_{rr}^{(i)}}, \quad t_1^{(i)} = \frac{\bar{C}_{z\theta}^{(i)} - \bar{C}_{zr}^{(i)}}{\bar{C}_{rr}^{(i)} - \bar{C}_{\theta\theta}^{(i)}} \tag{9a}$$

The integral constants $D_1^{(i)}$ and $D_2^{(i)}$ can be determined by boundary conditions, radial displacement and stress continuity conditions. Then the stresses are

$$\begin{aligned} \sigma_r^{(i)} &= d_1^{(i)} D_1^{(i)} r^{s_i - 1} + d_2^{(i)} D_2^{(i)} r^{-s_i - 1} + d_3^{(i)} \varepsilon_0 \\ \sigma_\theta^{(i)} &= d_4^{(i)} D_1^{(i)} r^{s_i - 1} + d_5^{(i)} D_2^{(i)} r^{-s_i - 1} + d_6^{(i)} \varepsilon_0 \\ \sigma_z^{(i)} &= d_7^{(i)} D_1^{(i)} r^{s_i - 1} + d_8^{(i)} D_2^{(i)} r^{-s_i - 1} + d_9^{(i)} \varepsilon_0 \end{aligned} \tag{10a}$$

where

$$\begin{aligned} &d_1^{(i)} = \bar{C}_{\theta r}^{(i)} + \bar{C}_{rr}^{(i)} s_i, \quad d_2^{(i)} = \bar{C}_{\theta r}^{(i)} - \bar{C}_{rr}^{(i)} s_i, \\ &d_3^{(i)} = \bar{C}_{zr}^{(i)} + \left(\bar{C}_{\theta r}^{(i)} + \bar{C}_{rr}^{(i)} \right) t_1^{(i)}, \quad d_4^{(i)} = \bar{C}_{\theta\theta}^{(i)} + \bar{C}_{\theta r}^{(i)} s_i, \\ &d_5^{(i)} = \bar{C}_{\theta\theta}^{(i)} - \bar{C}_{\theta r}^{(i)} s_i, \quad d_6^{(i)} = \bar{C}_{z\theta}^{(i)} + \left(\bar{C}_{\theta\theta}^{(i)} + \bar{C}_{\theta r}^{(i)} \right) t_1^{(i)}, \\ &d_7^{(i)} = \bar{C}_{z\theta}^{(i)} + \bar{C}_{zr}^{(i)} s_i, \quad d_8^{(i)} = \bar{C}_{z\theta}^{(i)} - \bar{C}_{zr}^{(i)} s_i, \\ &d_9^{(i)} = \bar{C}_{zz}^{(i)} + \left(\bar{C}_{z\theta}^{(i)} + \bar{C}_{zr}^{(i)} \right) t_1^{(i)}, \end{aligned}$$

When $s_i = 1$, it corresponds to isotropic material in r- θ plane; then, the solution of Eq. (9a) becomes

$$u_r^{(i)}(r) = D_1^{(i)} r + D_2^{(i)} / r + t_2^{(i)} \varepsilon_0 r \ln(r) \tag{8b}$$

where

$$t_2^{(i)} = \frac{\bar{C}_{z\theta}^{(i)} - \bar{C}_{zr}^{(i)}}{2\bar{C}_{rr}^{(i)}} \tag{9b}$$

Then, the stresses in Eq. (10a) become

$$\begin{aligned} \sigma_r^{(i)} &= d_1^{(i)} D_1^{(i)} + d_2^{(i)} D_2^{(i)} r^{-2} + \left(d_{31}^{(i)} + d_{32}^{(i)} \ln(r) \right) \varepsilon_0 \\ \sigma_\theta^{(i)} &= d_4^{(i)} D_1^{(i)} + d_5^{(i)} D_2^{(i)} r^{-2} + \left(d_{61}^{(i)} + d_{62}^{(i)} \ln(r) \right) \varepsilon_0 \\ \sigma_z^{(i)} &= d_7^{(i)} D_1^{(i)} + d_8^{(i)} D_2^{(i)} r^{-2} + \left(d_{91}^{(i)} + d_{92}^{(i)} \ln(r) \right) \varepsilon_0 \end{aligned} \tag{10b}$$

where

$$
\begin{aligned}
&d_1^{(i)} = \bar{C}_{\theta r}^{(i)} + \bar{C}_{rr}^{(i)}, \quad d_2^{(i)} = \bar{C}_{\theta r}^{(i)} - \bar{C}_{rr}^{(i)},\\
&d_4^{(i)} = \bar{C}_{\theta\theta}^{(i)} + \bar{C}_{\theta r}^{(i)}, \quad d_5^{(i)} = \bar{C}_{\theta\theta}^{(i)} - \bar{C}_{\theta r}^{(i)},\\
&d_7^{(i)} = \bar{C}_{z\theta}^{(i)} + \bar{C}_{zr}^{(i)}, \quad d_8^{(i)} = \bar{C}_{z\theta}^{(i)} - \bar{C}_{zr}^{(i)},\\
&d_{31}^{(i)} = \bar{C}_{zr}^{(i)} + \bar{C}_{rr}^{(i)} t_2^{(i)}, \quad d_{32}^{(i)} = \left(\bar{C}_{\theta r}^{(i)} + \bar{C}_{rr}^{(i)}\right) t_2^{(i)},\\
&d_{61}^{(i)} = \bar{C}_{z\theta}^{(i)} + \bar{C}_{\theta r}^{(i)} t_2^{(i)}, \quad d_{62}^{(i)} = \left(\bar{C}_{\theta\theta}^{(i)} + \bar{C}_{\theta r}^{(i)}\right) t_2^{(i)},\\
&d_{91}^{(i)} = \bar{C}_{zz}^{(i)} + \bar{C}_{zr}^{(i)} t_2^{(i)}, \quad d_{92}^{(i)} = \left(\bar{C}_{z\theta}^{(i)} + \bar{C}_{zr}^{(i)}\right) t_2^{(i)}
\end{aligned}
$$

2.4 Boundary and continuity conditions

The boundary conditions on the internal ($r = r_0$) and external ($r = r_n$) surfaces are given by

$$
\sigma_r^{(1)}|_{r=r_0} = -q_a, \quad \sigma_r^{(n)}|_{r=r_n} = 0 \tag{11a}
$$

At a given layer interface ($r = r_i$), the radial stress and displacement satisfy continuity conditions as

$$
\begin{aligned}
&\sigma_r^{(i)}|_{r=r_i} = \sigma_r^{(i+1)}|_{r=r_i},\\
&u_r^{(i)}(r_i) = u_r^{(i+1)}(r_i),
\end{aligned}
\quad (i = 1, 2, \ldots, n-1) \tag{11b}
$$

The equilibrium in z direction gives

$$
2\pi \sum_{i=1}^{n} \int_{r_{i-1}}^{r_i} \sigma_z^{(i)} r dr = q_a \pi r_0^2 \tag{11c}
$$

Above conditions in Eq. (11) lead to a set of equations, where the integral constants and axial strain are determined by

$$
[K]\{\delta\} = \{q_i\}
$$

$$
[K] = \begin{bmatrix}
a_{1,1} & a_{1,2} & \cdots & 0 & 0 & 0 & 0 & \cdots & 0 & 0 & a_{1,2n+1}\\
0 & 0 & \cdots & 0 & 0 & 0 & 0 & \cdots & a_{2,2n-1} & a_{2,2n} & a_{2,2n+1}\\
\cdots & \cdots & \cdots & \cdots & \cdots & \cdots & \cdots & \cdots & \cdots & \cdots & \cdots\\
0 & 0 & \cdots & a_{2i+1,2i-1} & a_{2i+1,2i} & a_{2i+1,2i+1} & a_{2i+1,2i+2} & \cdots & 0 & 0 & a_{2i+1,2n+1}\\
0 & 0 & \cdots & a_{2i+2,2i-1} & a_{2i+2,2i} & a_{2i+2,2i+1} & a_{2i+2,2i+2} & \cdots & 0 & 0 & a_{2i+2,2n+1}\\
\cdots & \cdots & \cdots & \cdots & \cdots & \cdots & \cdots & \cdots & \cdots & \cdots & \cdots\\
a_{2n+1,1} & a_{2n+1,2} & \cdots & a_{2n+1,2i-1} & a_{2n+1,2i} & a_{2n+1,2i+1} & a_{2n+1,2i+2} & \cdots & a_{2n+1,2n-1} & a_{2n+1,2n} & a_{2n+1,2n+1}
\end{bmatrix} \tag{12}
$$

In which nonzero elements in the stiffness matrix [K] are given as follows,

(1) Elements in the first two rows:

$$
\begin{aligned}
a_{1,1} &= \left(\bar{C}_{\theta r}^{(1)} + \bar{C}_{rr}^{(1)} s_1\right) r_0^{s_1-1} \\
a_{1,2} &= \left(\bar{C}_{\theta r}^{(1)} - \bar{C}_{rr}^{(1)} s_1\right) r_0^{-s_1-1} \\
a_{1,2n+1} &= \begin{cases} \bar{C}_{zr}^{(1)} + \left(\bar{C}_{\theta r}^{(1)} + \bar{C}_{rr}^{(1)}\right) \frac{\bar{C}_{z\theta}^{(1)} - \bar{C}_{zr}^{(1)}}{\bar{C}_{rr}^{(1)} - \bar{C}_{\theta\theta}^{(1)}}, & s_1 \neq 1 \\ \frac{\bar{C}_{z\theta}^{(1)} + \bar{C}_{zr}^{(1)}}{2} + \left(\bar{C}_{\theta r}^{(1)} + \bar{C}_{rr}^{(1)}\right) \frac{\bar{C}_{z\theta}^{(1)} - \bar{C}_{zr}^{(1)}}{2\bar{C}_{rr}^{(1)}} \ln(r_0), & s_1 = 1 \end{cases} \\
a_{2,2n-1} &= \left(\bar{C}_{\theta r}^{(n)} + \bar{C}_{rr}^{(n)} s_n\right) r_n^{s_n-1} \\
a_{2,2n} &= \left(\bar{C}_{\theta r}^{(n)} - \bar{C}_{rr}^{(n)} s_n\right) r_n^{-s_n-1} \\
a_{2,2n+1} &= \begin{cases} \bar{C}_{zr}^{(n)} + \left(\bar{C}_{\theta r}^{(n)} + \bar{C}_{rr}^{(n)}\right) \frac{\bar{C}_{z\theta}^{(n)} - \bar{C}_{zr}^{(n)}}{\bar{C}_{rr}^{(n)} - \bar{C}_{\theta\theta}^{(n)}}, & s_n \neq 1 \\ \frac{\bar{C}_{z\theta}^{(n)} + \bar{C}_{zr}^{(n)}}{2} + \left(\bar{C}_{\theta r}^{(n)} + \bar{C}_{rr}^{(n)}\right) \frac{\bar{C}_{z\theta}^{(n)} - \bar{C}_{zr}^{(n)}}{2\bar{C}_{rr}^{(n)}} \ln r_{n-1}, & s_n = 1 \end{cases}
\end{aligned}
$$

(2) Elements from the third row to the second row from bottom, in which loop index $i = 1, 2, \ldots, n-1$.

$$
\begin{aligned}
a_{2i+1,2i-1} &= \left(\bar{C}_{\theta r}^{(i)} + \bar{C}_{rr}^{(i)} s_i\right) r_i^{s_i-1}, \\
a_{2i+1,2i} &= \left(\bar{C}_{\theta r}^{(i)} - \bar{C}_{rr}^{(i)} s_i\right) r_i^{-s_i-1}, \\
a_{2i+1,2i+1} &= -\left(\bar{C}_{\theta r}^{(i+1)} + \bar{C}_{rr}^{(i+1)} s_{i+1}\right) r_i^{s_{i+1}-1}, \qquad (i = 1, 2, \ldots, n-1) \\
a_{2i+1,2i+2} &= -\left(\bar{C}_{\theta r}^{(i+1)} - \bar{C}_{rr}^{(i+1)} s_{i+1}\right) r_i^{-s_{i+1}-1}
\end{aligned}
$$

$$
\begin{aligned}
a_{2i+1,2n+1} &= e_3^{(i)} - e_4^{(i)}, \quad (i = 1, 2, \ldots, n-1) \\
e_3^{(i)} &= \begin{cases} \bar{C}_{zr}^{(i)} + \left(\bar{C}_{\theta r}^{(i)} + \bar{C}_{rr}^{(i)}\right) \frac{\bar{C}_{z\theta}^{(i)} - \bar{C}_{zr}^{(i)}}{\bar{C}_{rr}^{(i)} - \bar{C}_{\theta\theta}^{(i)}}, & s_i \neq 1 \\ \frac{\bar{C}_{z\theta}^{(i)} + \bar{C}_{zr}^{(i)}}{2} + \left(\bar{C}_{\theta r}^{(i)} + \bar{C}_{rr}^{(i)}\right) \frac{\bar{C}_{z\theta}^{(i)} - \bar{C}_{zr}^{(i)}}{2\bar{C}_{rr}^{(i)}} \ln r_i, & s_i = 1 \end{cases} \\
e_4^{(i)} &= \begin{cases} \bar{C}_{zr}^{(i+1)} + \left(\bar{C}_{\theta r}^{(i+1)} + \bar{C}_{rr}^{(i+1)}\right) \frac{\bar{C}_{z\theta}^{(i+1)} - \bar{C}_{zr}^{(i+1)}}{\bar{C}_{rr}^{(i+1)} - \bar{C}_{\theta\theta}^{(i+1)}}, & s_{i+1} \neq 1 \\ \frac{\bar{C}_{z\theta}^{(i+1)} + \bar{C}_{zr}^{(i+1)}}{2} + \left(\bar{C}_{\theta r}^{(i+1)} + \bar{C}_{rr}^{(i+1)}\right) \frac{\bar{C}_{z\theta}^{(i+1)} - \bar{C}_{zr}^{(i+1)}}{2\bar{C}_{rr}^{(i+1)}} \ln r_i, & s_{i+1} = 1 \end{cases} \\
a_{2i+2,2i-1} &= r_i^{s_i-1}, \\
a_{2i+2,2i} &= r_i^{-s_i-1} \\
a_{2i+2,2i+1} &= -r_i^{s_{i+1}-1} \\
a_{2i+2,2i+2} &= -r_i^{-s_{i+1}-1} \\
a_{2i+2,2n+1} &= e_5^{(i)} - e_6^{(i)}, \quad (i = 1, 2, \ldots, n-1) \\
e_5^{(i)} &= \begin{cases} \frac{\bar{C}_{z\theta}^{(i)} - \bar{C}_{zr}^{(i)}}{\bar{C}_{rr}^{(i)} - \bar{C}_{\theta\theta}^{(i)}}, & s_i \neq 1 \\ \frac{\bar{C}_{z\theta}^{(i)} - \bar{C}_{zr}^{(i)}}{2\bar{C}_{rr}^{(i)}} \ln r_i, & s_i = 1 \end{cases} \\
e_6^{(i)} &= \begin{cases} \frac{\bar{C}_{z\theta}^{(i+1)} - \bar{C}_{zr}^{(i+1)}}{\bar{C}_{rr}^{(i+1)} - \bar{C}_{\theta\theta}^{(i+1)}}, & s_{i+1} \neq 1 \\ \frac{\bar{C}_{z\theta}^{(i+1)} - \bar{C}_{zr}^{(i+1)}}{2\bar{C}_{rr}^{(i+1)}} \ln r_i, & s_{i+1} = 1 \end{cases}
\end{aligned}
$$

(3) Elements in the last row:

$$a_{2n+1,2i-1} = \frac{2\left(\bar{C}_{z\theta}^{(i)}+\bar{C}_{zr}^{(i)}s_i\right)\left(r_i^{s_i+1}-r_{i-1}^{s_i+1}\right)}{1+s_i},$$

$$a_{2n+1,2i} = \begin{cases} \dfrac{2\left(\bar{C}_{z\theta}^{(i)}-\bar{C}_{zr}^{(i)}s_i\right)\left(r_i^{1-s_i}-r_{i-1}^{1-s_i}\right)}{1-s_i}, & s_i \neq 1 \\ 2\left(\bar{C}_{z\theta}^{(i)}-\bar{C}_{zr}^{(i)}\right)\ln(r_i/r_{i-1}), & s_i = 1 \end{cases}, \quad (i = 1, 2, \ldots, n)$$

$$a_{2n+1,2n+1} = \sum_{i=1}^{n} e_7^{(i)}$$

$$e_7^{(i)} = \begin{cases} \left[\bar{C}_{zz}^{(i)} + \left(\bar{C}_{z\theta}^{(i)}+\bar{C}_{zr}^{(i)}\right)\dfrac{\bar{C}_{z\theta}^{(i)}-\bar{C}_{zr}^{(i)}}{\bar{C}_{rr}^{(i)}-\bar{C}_{\theta\theta}^{(i)}}\right]\left(r_i^2-r_{i-1}^2\right), & s_i \neq 1 \\ \left[\bar{C}_{zz}^{(i)} - \dfrac{\left(\bar{C}_{z\theta}^{(i)}-\bar{C}_{zr}^{(i)}\right)^2}{4\bar{C}_{rr}^{(i)}}\right]\left(r_i^2-r_{i-1}^2\right) + \dfrac{\bar{C}_{z\theta}^{(i)2}-\bar{C}_{zr}^{(i)2}}{2\bar{C}_{rr}^{(i)}}\left(r_i^2\ln r_i - r_{i-1}^2\ln r_{i-1}\right), & s_i = 1 \end{cases} \quad (i = 1, 2, \ldots, n)$$

(4) Vector of unknown integral constants and loading parameters:

$$\{\delta\} = \left\{D_1^{(1)}, D_2^{(1)}, \ldots, D_1^{(i)}, D_2^{(i)}, \ldots, D_1^{(n)}, D_2^{(n)}, \varepsilon_0\right\}^T$$

$$\{q_i\} = \left\{-q_a, 0, 0, \ldots, 0, q_a r_0^2\right\}^T$$

Solving Eq. (12), the displacements, strains and the stresses of each layer can be determined.

2.5 3-D stresses in fiber directions

The stresses in Eq. (10) are average values in each orthotropic layer in global coordinate system. Stresses in fiber directions such as longitudinal stress $\sigma_1^{(i)}$, transverse stresses $\sigma_2^{(i)}$, $\sigma_3^{(i)}$ and shear stress $\tau_{12}^{(i)}$ in fiber layer can be determined by on-axis stress–strain relation. First, we need on-axis strains by coordinate transformation of off-axis. From deformations in Eq. (8) and strain definition, we can get strains in cylindrical coordinate system. Then the on-axis strains can be obtained with coordinate transformation of strains. Finally, the stresses in fiber directions are derived as

$$\begin{aligned}
\sigma_1^{(i)} &= \left(n_i^2 C_{11}^{(i)} + m_i^2 C_{12}^{(i)} + s_i C_{13}^{(i)}\right) D_1^{(i)} r^{s_i-1} \\
&\quad + \left(n_i^2 C_{11}^{(i)} + m_i^2 C_{12}^{(i)} - s_i C_{13}^{(i)}\right) D_2^{(i)} r^{-s_i-1} \\
&\quad + \left[C_{11}^{(i)}\left(m_i^2 + n_i^2 t_1^{(i)}\right) + C_{12}^{(i)}\left(n_i^2 + m_i^2 t_1^{(i)}\right) + C_{13}^{(i)} t_1^{(i)}\right]\varepsilon_0 \\
\sigma_2^{(i)} &= \left(n_i^2 C_{12}^{(i)} + m_i^2 C_{22}^{(i)} + s_i C_{23}^{(i)}\right) D_1^{(i)} r^{s_i-1} \\
&\quad + \left(n_i^2 C_{12}^{(i)} + m_i^2 C_{22}^{(i)} - s_i C_{23}^{(i)}\right) D_2^{(i)} r^{-s_i-1} \\
&\quad + \left[C_{12}^{(i)}\left(m_i^2 + n_i^2 t_1^{(i)}\right) + C_{22}^{(i)}\left(n_i^2 + m_i^2 t_1^{(i)}\right) + C_{23}^{(i)} t_1^{(i)}\right]\varepsilon_0 \\
\sigma_3^{(i)} &= \left(n_i^2 C_{13}^{(i)} + m_i^2 C_{23}^{(i)} + s_i C_{33}^{(i)}\right) D_1^{(i)} r^{s_i-1} \\
&\quad + \left(n_i^2 C_{13}^{(i)} + m_i^2 C_{23}^{(i)} - s_i C_{33}^{(i)}\right) D_2^{(i)} r^{-s_i-1} \\
&\quad + \left[C_{13}^{(i)}\left(m_i^2 + n_i^2 t_1^{(i)}\right) + C_{23}^{(i)}\left(n_i^2 + m_i^2 t_1^{(i)}\right) + C_{33}^{(i)} t_1^{(i)}\right]\varepsilon_0 \\
\tau_{12}^{(i)} &= 2m_i n_i G_{12}\left[D_1^{(i)} r^{s_i-1} + D_2^{(i)} r^{-s_i-1} + (t_1^{(i)} - 1)\varepsilon_0\right]
\end{aligned} \tag{13a}$$

when $s_i = 1$, stresses in fiber directions become

$$\begin{aligned}
\sigma_1^{(i)} &= \left(n_i^2 C_{11}^{(i)} + m_i^2 C_{12}^{(i)} + C_{13}^{(i)}\right) D_1^{(i)} \\
&\quad + \left(n_i^2 C_{11}^{(i)} + m_i^2 C_{12}^{(i)} - C_{13}^{(i)}\right) D_2^{(i)}/r^2 \\
&\quad + \left[C_{11}^{(i)}\left(m_i^2 + n_i^2 t_2^{(i)} \ln r\right) + C_{12}^{(i)}\left(n_i^2 + m_i^2 t_2^{(i)} \ln r\right) + C_{13}^{(i)} t_2^{(i)}(1 + \ln r)\right]\varepsilon_0 \\
\sigma_2^{(i)} &= \left(n_i^2 C_{12}^{(i)} + m_i^2 C_{22}^{(i)} + C_{23}^{(i)}\right) D_1^{(i)} \\
&\quad + \left(n_i^2 C_{12}^{(i)} + m_i^2 C_{22}^{(i)} - C_{23}^{(i)}\right) D_2^{(i)}/r^2 \\
&\quad + \left[C_{12}^{(i)}\left(m_i^2 + n_i^2 t_2^{(i)} \ln r\right) + C_{22}^{(i)}\left(n_i^2 + m_i^2 t_2^{(i)} \ln r\right) + C_{23}^{(i)} t_2^{(i)}(1 + \ln r)\right]\varepsilon_0 \\
\sigma_3^{(i)} &= \left(n_i^2 C_{13}^{(i)} + m_i^2 C_{23}^{(i)} + C_{33}^{(i)}\right) D_1^{(i)} \\
&\quad + \left(n_i^2 C_{13}^{(i)} + m_i^2 C_{23}^{(i)} - C_{33}^{(i)}\right) D_2^{(i)}/r^2 \\
&\quad + \left[C_{13}^{(i)}\left(m_i^2 + n_i^2 t_2^{(i)} \ln r\right) + C_{23}^{(i)}\left(n_i^2 + m_i^2 t_2^{(i)} \ln r\right) + C_{33}^{(i)} t_2^{(i)}(1 + \ln r)\right]\varepsilon_0 \\
\tau_{12}^{(i)} &= 2 m_i n_i G_{12}\left[D_1^{(i)} + D_2^{(i)}/r^2 + (t_2^{(i)} \ln r - 1)\varepsilon_0\right]
\end{aligned} \tag{13b}$$

3 Optimization model and method

3.1 Failure criteria

Composite material failure criterions are the maximum stress criterion, the maximum strain criterion, Tsai–Hill criteria, Hoffman criteria, and Tsai–Wu criterion. Here three-dimensional Tsai–Wu failure criterion is adopted in strength ratio calculation. The failure surface of Tsai–Wu criterion is [25]:

$$-F_{zz}\sigma_1^2 - F_{rr}\left(\sigma_2^2 + \sigma_3^2\right) + F_{ss}\tau_{12}^2 + 2F_{rz}\left(\sigma_2 + \sigma_3\right)\sigma_1 + 2F_{r\theta}\sigma_2\sigma_3 + F_r(\sigma_2 + \sigma_3) + F_z\sigma_1 = 1 \tag{14}$$

where

$$\begin{aligned}
&F_{zz} = 1/(X_t X_c),\ F_{rr} = 1/(Y_t Y_c),\ \ F_{ss} = 1/S^2, \\
&F_{rz} = -0.5/\sqrt{X_t X_c Y_t Y_c},\ \ F_{r\theta} = 1/(2Y_t Y_c), \\
&F_r = 1/Y_t + 1/Y_c,\ \ F_z = 1/X_t + 1/X_c
\end{aligned}$$

In which X_t, X_c represent the longitudinal tensile strength and compression strength in fiber directions, respectively. Y_t, Y_c are the fiber transverse tensile strength and compression strength, respectively. S is the shear strength. σ_1 is the longitudinal stress in fiber direction. σ_2 and σ_3 are the transversed stresses. τ_{12} is the shear stress.

3.2 Strength ratio calculation

From Eq. (14), we calculate the strength ratio by

$$R = -\xi/(2\rho) + \sqrt{\xi^2/(2\rho)^2 + 1/\rho} \tag{15}$$

In which

$$\begin{aligned}
\rho &= -F_{zz}\sigma_1^2 - F_{rr}\left(\sigma_2^2 + \sigma_3^2\right) + F_{ss}\tau_{12}^2 \\
&\quad + 2F_{rz}(\sigma_2 + \sigma_3)\sigma_1 + 2F_{r\theta}\sigma_2\sigma_3, \\
\xi &= F_r(\sigma_2 + \sigma_3) + F_z\sigma_1
\end{aligned} \qquad \text{(Tsai-Wu criterion)}$$

3.3 Optimization method

We used two methods, complex method (CM) and steepest descent (SD) to find the optimization solution [26].

3.3.1 Complex method

Actually, CM is a development of simplex method in constrained problems. In 1965, Box extended the simplex method of unconstrained minimization to solve constrained minimization problems of nonlinear programming:

$$\text{Minimize } f(X) \tag{16a}$$

subject to

$$g_j(X) \leq 0, \quad (j = 1, 2, \ldots, m) \tag{16b}$$

$$x_i^{(l)} \leq x_i \leq x_i^{(u)}, \quad (i = 1, 2, \ldots, n) \tag{16c}$$

In general, the satisfaction of the side constraints (lower and upper bounds on the variables x_i) may not correspond to the satisfaction of the constraints $g_j(\boldsymbol{X}) \leq 0$. The formation of a sequence of geometric figures each having $k = n + 1$ vertices in an n-dimensional space (called the simplex) is the basic idea, where a sequence of geometric figures each having $k \geq n + 1$ vertices is formed to find the constrained minimum point. The method assumes that an initial feasible point $\boldsymbol{X}_1$ (which satisfies all the m constraints) is available. **Iterative steps in the procedure:**

(1) Find $k \geq n + 1$ points, satisfied all m constraints.
(2) The objective function is evaluated at each of the k points (vertices). If the vertex $\boldsymbol{X}_h$ corresponds to the largest function value, the reflection is used to find a new point $\boldsymbol{X}_r$ as

$$X_r = X_0 + \alpha(X_0 - X_h) \tag{17}$$

where $\alpha = 1.3$ and $\boldsymbol{X}_0$ is the centroid of all vertices except $\boldsymbol{X}_h$:

$$X_0 = \frac{1}{k-1} \sum_{\substack{l=1 \\ l \neq k}}^{k} X_l \tag{18}$$

(3) If the point $\boldsymbol{X}_r$ is feasible and $f(\boldsymbol{X}_r) < f(\boldsymbol{X}_h)$, then point $\boldsymbol{X}_h$ is replaced by $\boldsymbol{X}_r$, and turn to step 2. If $f(\boldsymbol{X}_r) \geq f(\boldsymbol{X}_h)$, a new trial point $\boldsymbol{X}_r$ is found by reducing the value of α in Eq. (16) by a factor of 2 and is tested for the satisfaction of the relation $f(\boldsymbol{X}_r) < f(\boldsymbol{X}_h)$. The procedure of finding a new point $\boldsymbol{X}_r$ with a reduced value of α is repeated again. This procedure is repeated, until the value of α becomes very small. If an improved point $\boldsymbol{X}_r$, with $f(\boldsymbol{X}_r) < f(\boldsymbol{X}_h)$, cannot be obtained even with that small value of α, the point $\boldsymbol{X}_r$ is discarded and the entire procedure of the reflection is restarted by using the point $\boldsymbol{X}_p$ (which has the second-highest function value) instead of $\boldsymbol{X}_h$.
(4) If at any stage, the reflected point $\boldsymbol{X}_r$ (found in step 3) violates any of the constraints, it is moved halfway in toward the centroid until it becomes feasible. This method will progress toward the optimum point as long as the complex has not collapsed into its centroid.
(5) Each time the worst point $\boldsymbol{X}_h$ of the current complex is replaced by a new point, the complex gets modified, and we have to test for the convergence of the process. We assume convergence of the process whenever the following two conditions are satisfied:
   (a) The complex shrinks to a specified small size.
   (b) The standard deviation of the function value becomes sufficiently small.

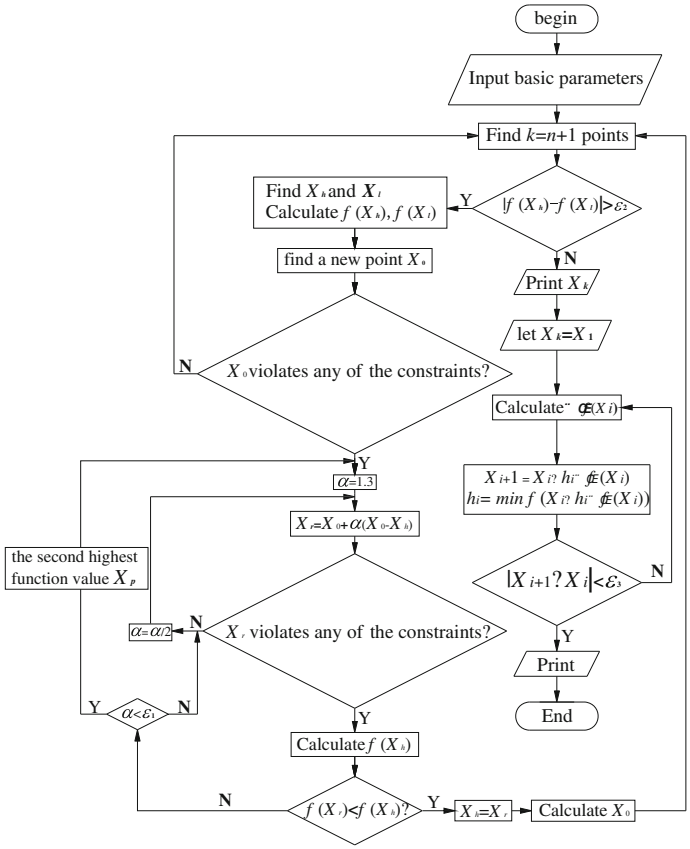

Fig. 2 Combined method diagram

Table 1 Material property of winding filaments [24,25,27]

Material	E-glass/epoxy	T300/934	T300/5208
E_1 (GPa)	43.4	141.6	181
E_2 (GPa)	15.2	10.7	10.3
ν_{21}	0.29	0.268	7.17
ν_{32}	0.38	0.495	0.30
G_{12} (GPa)	6.14	3.88	0.28
X_t (MPa)	1062	1314	1500
X_c (MPa)	610	1220	1500
Y_t (MPa)	31	43	40
Y_c (MPa)	118	168	246
S (MPa)	72	48	68

3.3.2 Steepest descent method

SD is one of the simplest and the most fundamental minimization methods for unconstrained optimization. Since it uses the negative gradient as its descent direction, it is also called the gradient method. It can be summarized by the following steps:

(1) Start with an arbitrary initial point $\boldsymbol{X}_1$. Set the iteration number as $i = 1$.
(2) Find the search direction $\nabla f(\boldsymbol{X}_i)$.
(3) Determine the optimal step length h_i in the direction $\nabla f(\boldsymbol{X}_i)$, and set

$$X_i + 1 = X_i - h_i \nabla f(X_i) \tag{19}$$

(4) Test the new point, $\boldsymbol{X}_{i+1}$, for optimality. If $\boldsymbol{X}_{i+1}$ is optimum, stop the process. Otherwise, go to next step.
(5) Set the new iteration number $i = i + 1$, and return to step 2.

Table 2 Optimized winding angle of T300/934 (°)

$\frac{r_0/r_n}{n}$	0.95	0.90	0.85	0.80	0.75	0.70	0.65
1	52.758	57.531	64.373	73.422	81.301	80.557	81.803
2	45.761	49.312	55.391	89.270	89.838	89.579	88.555
3	51.568	43.095	52.159	85.899	89.948	89.349	88.300
4	50.134	58.671	56.848	57.292	86.413	87.844	84.567
5	61.725	56.062	46.404	57.222	59.014	58.957	63.583
6	52.202	48.825	43.293	34.623	0.0338	0.0460	24.685
7	54.015	51.218	53.971	31.640	44.242	36.323	0.0058
8	56.142	54.655	52.146	52.724	41.705	89.070	49.339
9	58.664	59.654	63.949	36.562	45.198	24.226	89.881
10	61.709	67.504	64.373	49.647	35.316	34.279	13.092

Table 3 Optimized winding angle of E-glass/epoxy(°)

$\frac{r_0/r_n}{n}$	0.95	0.90	0.85	0.80	0.75	0.70	0.65
1	54.895	54.459	56.895	61.863	58.310	62.952	66.241
2	56.584	54.860	54.402	56.552	56.453	59.970	61.200
3	57.448	55.365	54.466	55.233	66.462	66.587	74.538
4	56.026	58.566	58.989	59.876	55.058	56.263	69.249
5	56.438	60.731	55.553	55.655	54.098	55.090	53.227
6	56.885	57.873	57.546	56.396	56.606	54.510	57.324
7	57.365	60.937	62.669	57.564	55.205	55.351	51.614
8	57.880	60.273	59.244	59.225	56.506	57.253	52.969
9	62.518	63.832	65.852	62.296	66.329	62.932	56.100
10	72.083	73.627	63.224	64.873	62.583	71.389	62.157

Table 4 Optimized winding angle of (a) T300/934 (°), (b) E-glass/epoxy (°)

$\frac{r_0/r_n}{n}$	0.95	0.90	0.85	0.80	0.75	0.70	0.65
(a) T300/934 (°)							
1	54.575	54.681	54.791	55.900	56.208	56.539	56.903
1	48.738	48.867	60.176	70.348	89.999	89.997	89.998
2	53.253	48.070	40.589	51.313	89.995	89.996	89.992
3	62.701	65.195	61.611	45.069	0.005	0.005	0.005
1	48.738	50.813	67.756	70.185	89.999	89.999	89.999
2	50.716	49.177	52.064	71.055	89.999	89.995	89.995
3	53.253	50.014	43.773	52.124	89.999	89.996	89.995
4	57.023	55.095	45.746	36.836	29.075	30.096	29.530
5	62.701	66.845	62.451	47.653	0.005	0.0007	0.009
1	48.738	51.876	70.127	70.772	89.999	89.995	89.995
2	49.591	50.783	62.555	75.141	89.999	89.998	89.999
3	50.481	50.125	56.118	72.987	89.999	89.995	89.995
4	51.466	49.999	51.030	66.438	89.999	89.995	89.995
5	52.606	50.518	47.528	57.573	89.999	89.995	89.995
6	53.960	51.792	45.878	48.426	89.921	89.999	89.995
7	55.587	53.937	46.377	40.946	46.124	49.278	49.468
8	57.547	57.075	49.354	37.066	0.305	0.0173	0.0063
9	59.899	61.340	55.191	38.745	0.0003	0.0044	0.0051
10	62.701	67.661	64.730	48.413	0.0001	0.0059	0.00001
1	48.799	52.265	81.073	73.361	25.379	32.042	33.739
2	49.086	51.695	75.460	82.268	89.999	87.820	87.152
3	49.572	51.210	64.096	82.163	89.942	88.704	86.384
4	49.969	50.820	58.908	81.352	89.999	89.999	85.830
5	50.290	50.538	53.967	73.679	89.999	89.999	84.952
6	50.845	50.375	51.302	64.094	89.999	89.999	83.200
7	51.346	50.343	48.948	58.781	89.999	89.999	80.240
8	51.806	50.454	47.935	54.193	89.999	88.702	75.952

Table 4 continued

$\frac{r_0/r_n}{n}$	0.95	0.90	0.85	0.80	0.75	0.70	0.65
9	52.434	50.721	47.294	54.682	89.999	83.727	70.460
10	52.944	51.153	48.057	53.482	87.917	76.767	64.063
11	53.646	51.765	47.257	53.140	78.461	68.218	57.158
12	54.253	52.568	46.926	51.436	65.984	58.701	50.175
13	55.063	53.573	47.097	47.173	52.550	48.898	43.505
14	55.831	54.794	47.802	43.633	39.688	39.435	37.509
15	56.826	56.242	49.075	40.886	28.204	30.819	32.487
16	57.785	57.931	50.953	39.250	18.767	23.515	28.706
17	58.886	59.873	53.470	38.903	11.922	17.911	26.397
18	59.994	62.081	56.667	39.988	7.786	14.275	25.750
19	61.277	64.569	60.586	42.711	5.837	12.818	27.002
20	62.667	67.919	66.843	47.863	5.922	13.644	30.489
(b) E-glass/epoxy (°)							
1	58.864	58.722	58.574	58.420	58.259	59.921	63.270
1	57.111	55.989	55.118	57.047	58.280	61.473	67.083
2	58.853	59.594	58.945	56.602	54.738	52.611	53.046
3	61.460	67.583	69.668	66.742	74.392	78.684	65.808
1	56.935	55.989	55.662	57.319	59.445	63.400	68.203
2	57.838	57.461	56.486	56.275	57.042	58.123	59.398
3	58.887	59.594	59.060	56.860	56.245	54.485	54.252
4	60.117	62.825	62.727	60.111	60.790	59.113	55.451
5	61.505	67.583	70.174	66.744	74.948	79.354	66.454
1	56.877	56.030	56.005	57.517	60.123	64.932	68.835
2	57.071	56.578	56.305	56.900	58.954	61.332	64.622
3	57.501	57.249	56.709	56.514	57.862	58.968	60.842
4	57.965	58.071	57.313	56.435	57.018	57.263	57.720
5	58.464	59.049	58.232	56.739	56.731	56.145	55.618
6	59.072	60.202	59.550	57.528	57.348	56.075	54.519
7	59.739	61.612	61.277	58.831	59.087	57.606	54.799
8	60.401	63.299	63.611	60.707	62.356	60.677	56.695
9	61.024	65.288	66.627	63.299	67.452	67.100	60.453
10	61.594	67.612	70.437	66.741	75.086	80.460	66.500
1	56.899	56.126	56.240	57.674	60.270	64.447	69.038
2	57.057	56.290	56.229	57.188	59.568	63.052	66.503
3	57.113	56.524	56.327	56.867	58.684	61.814	64.238
4	57.158	56.822	56.470	56.808	58.463	60.638	62.402
5	57.280	57.203	56.612	56.690	58.297	59.211	61.104
6	57.497	57.584	56.896	56.560	58.036	58.338	59.511
7	57.728	57.937	57.269	56.435	57.721	57.554	58.205
8	57.992	58.335	57.776	56.547	57.888	57.126	57.167
9	58.308	58.828	58.060	56.663	58.082	56.717	56.382
10	58.644	59.396	58.768	56.971	57.843	56.795	55.833
11	58.990	59.907	59.241	57.297	57.709	56.624	55.507
12	59.334	60.529	60.032	57.752	57.722	57.169	55.392
13	59.665	61.180	60.889	58.374	58.403	57.896	55.475
14	59.972	61.919	61.743	59.346	60.070	58.771	55.748
15	60.243	62.695	62.769	60.085	61.169	59.758	56.198
16	60.468	63.683	63.887	60.896	62.186	61.825	56.819
17	60.635	64.569	65.155	62.078	64.320	63.944	57.601
18	61.033	65.582	66.750	63.447	66.820	66.068	59.535
19	61.251	66.647	68.425	64.982	69.811	70.202	61.883
20	61.678	67.842	70.528	66.578	74.196	75.971	65.100

3.3.3 The combined method

In order to improve the efficiency of above methods, a combined complex–steepest descent method is developed to achieve better results. The process of the calculation is: first, we use CM to find an optimized winding angle sequence, then curve fit the results to obtain a more smooth distribution of winding angle sequence, and finally, optimize the fitted curve with SD. The combined method diagram is given in Fig. 2.

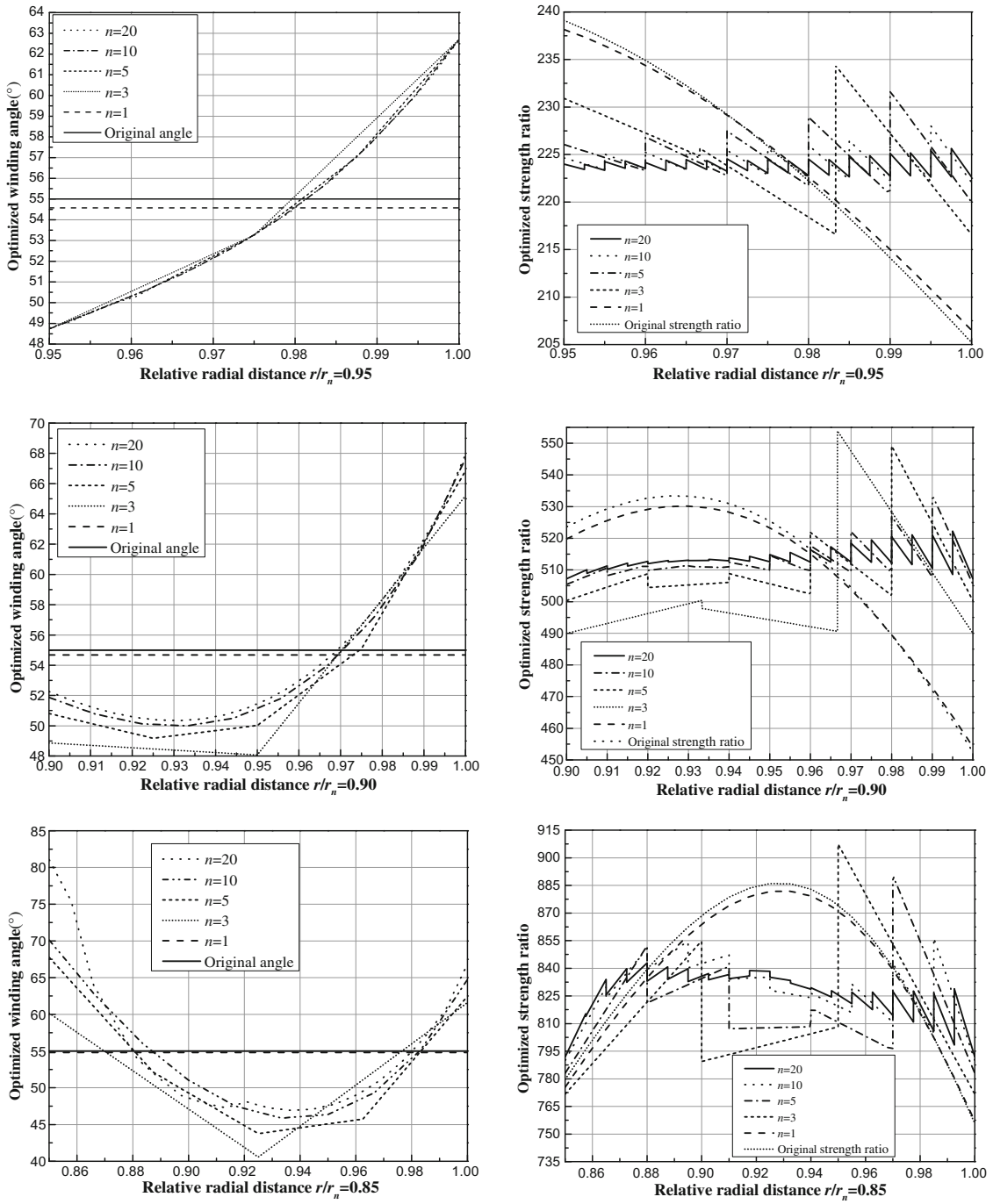

Fig. 3 The optimized winding angle and the corresponding strength ratio distributions via thickness of T300/934

3.4 Optimized winding angle sequence

Here carbon fiber epoxy (T300/934) and E-glass/epoxy are used, whose properties are listed in Table 1.

Under 0.1111111 MPa internal pressure, letting $n = 1$, it describes a uniform winding angle cylinder. Letting $n = 1, 3, 5, 10, 20$, multi-angle FW cylinder with different number of winding angle sequence for ratio of the inner radius to outer radius $r_0/r_n = 0.95, 0.90, 0.85, 0.80, 0.75, 0.70, 0.65$ is simulated.

To get the optimal variation of winding angles sequence, we used CM, SD and a combined complex–steepest descent method to solve the problem.

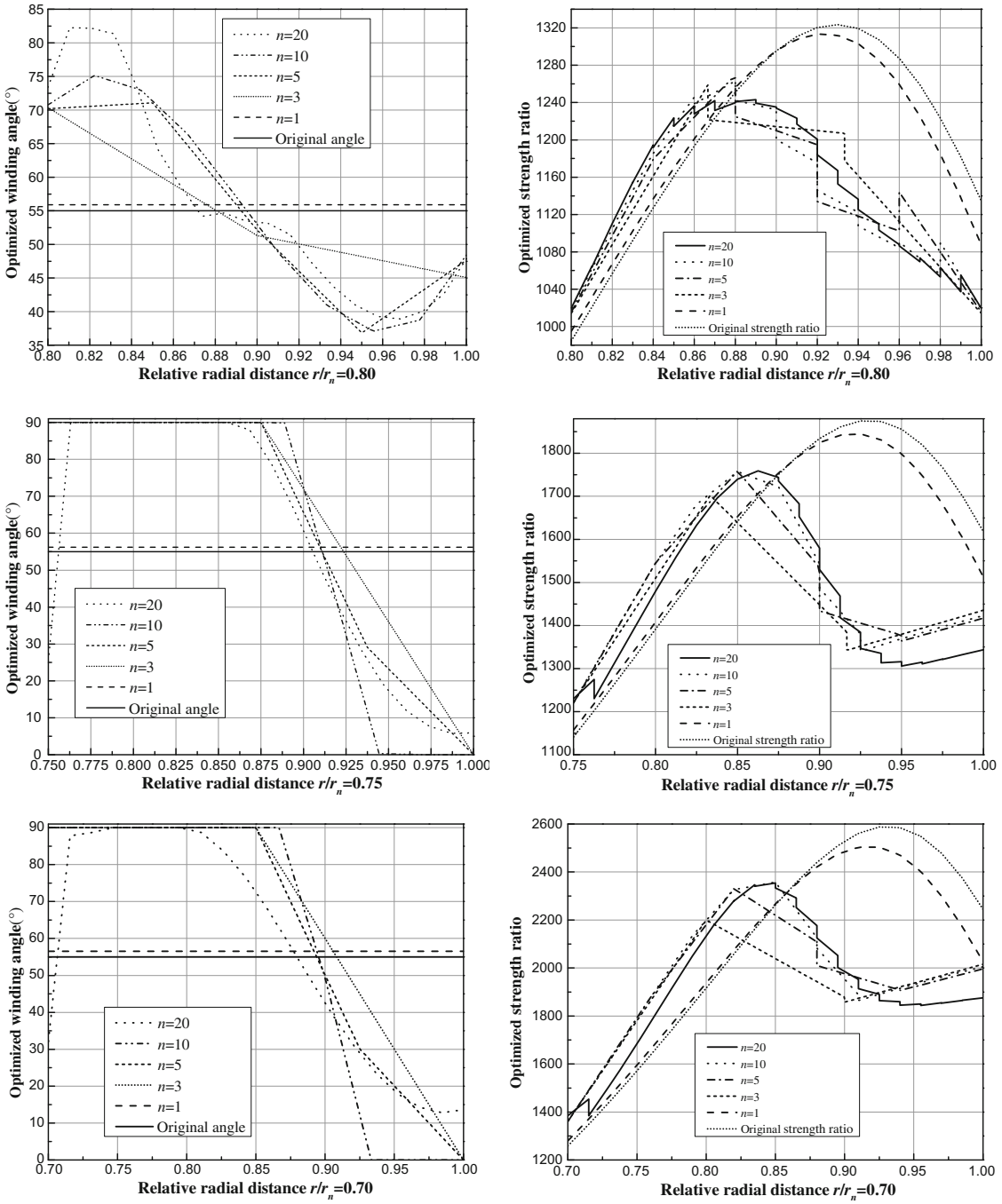

Fig. 3 continued

3.4.1 Results of CM

For a series multi-layered T300/934 cylinders and E-glass/epoxy cylinders, the optimized winding angle is obtained with CM.

For different radius ratio cylindrical vessels, it is found that the variation of the optimized winding angle is unstable and fluctuating for large number of n. This result makes the distributions of strength ratio via thickness are also unstable and fluctuating, so the maximum strength ratio and more uniform strength for all layers cannot be achieved. For example, a T300/934 cylinder ($n = 10$), the results were obtained and given in Table 2.

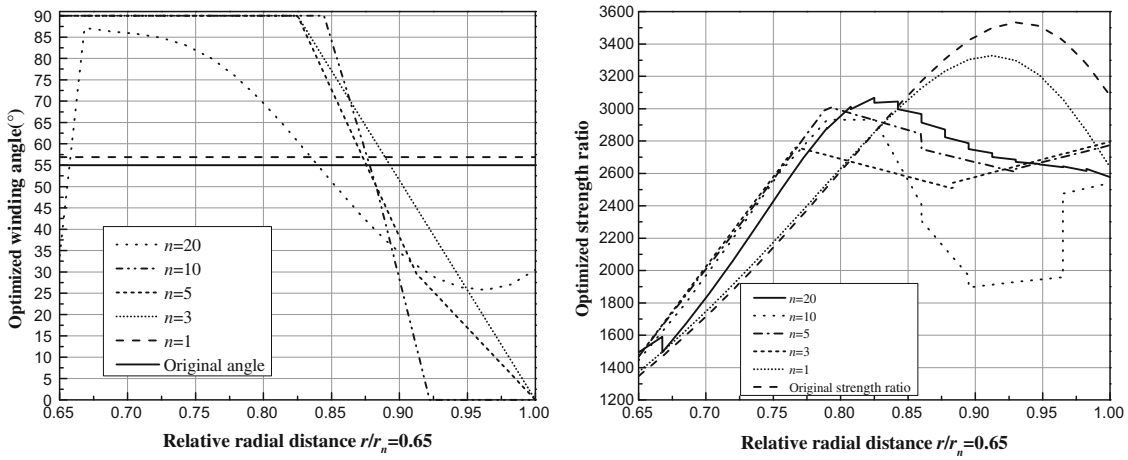

Fig. 3 continued

Table 5 The strength ratio in 20-layer cylinder of original and optimized winding angle of (a) T300/934

r_0/r_n	Original winding angle				Optimized winding angle			
	Maximum	Minimum	D-value	Performance (%)	Maximum	Minimum	D-value	Performance (%)
0.95	239.114	205.204	33.910	14.18	225.640	222.639	3.001	1.17
0.90	533.356	452.496	80.860	15.16	522.258	507.212	15.046	2.88
0.85	885.986	755.753	130.233	14.70	842.930	791.887	51.043	6.06
0.80	1323.426	984.517	338.909	25.61	1243.018	1019.579	223.439	17.98
0.75	1874.700	1141.303	733.397	39.12	1758.986	1230.130	528.856	30.07
0.70	2587.480	1259.050	1328.430	51.34	2354.651	1384.064	970.587	41.22
0.65	3533.295	1346.453	2186.842	61.90	3067.299	1493.992	1573.307	51.29

3.4.2 Results of SD

With SD, the results with the same geometric parameters for T300/934 cylinders and E-glass/epoxy cylinders are given.

From the results, we find that the optimized winding angle sequences are smooth, but the strength ratios do not achieve the optimal state, so the maximum strength ratio is not achieved. For example, a E-glass/epoxy cylinder ($n = 10$), the results are obtained and given in Table 3.

3.4.3 Results of the combined method

The optimization study shows that the optimized winding angle sequences tend to unique distribution of winding angle when the layer number n goes to large number and the lowest strength ratio achieves the optimal level.

For T300/934 cylinders and E-glass/epoxy cylinders with different radius ratio r_0/r_n and layer numbers n, the results are obtained with the combined method and listed in Table 4(a,b), respectively.

From the results, we find that the variation of the optimized winding angle is stable and smooth for large number of n, and the strength ratios achieve the optimal state. More details will be discussed in the next section.

4 Discussion of the results

Choose the combined method and different radius ratio $r_0/r_n = 0.95, 0.90, 0.85, 0.80, 0.75, 0.70, 0.65$, etc., the winding angle sequence to maximize the lowest strength ratio is optimized. We choose layer number $n = 1, 3, 5, 10$ and 20, to simulate the winding angle variation for the optimized scheme of infinite thin thickness of winding layer. For a single-angle winding thin-walled cylinder, the optimized winding angle is about 55° [7–11]. So $\phi = 55°$ is chosen as the original winding angle.

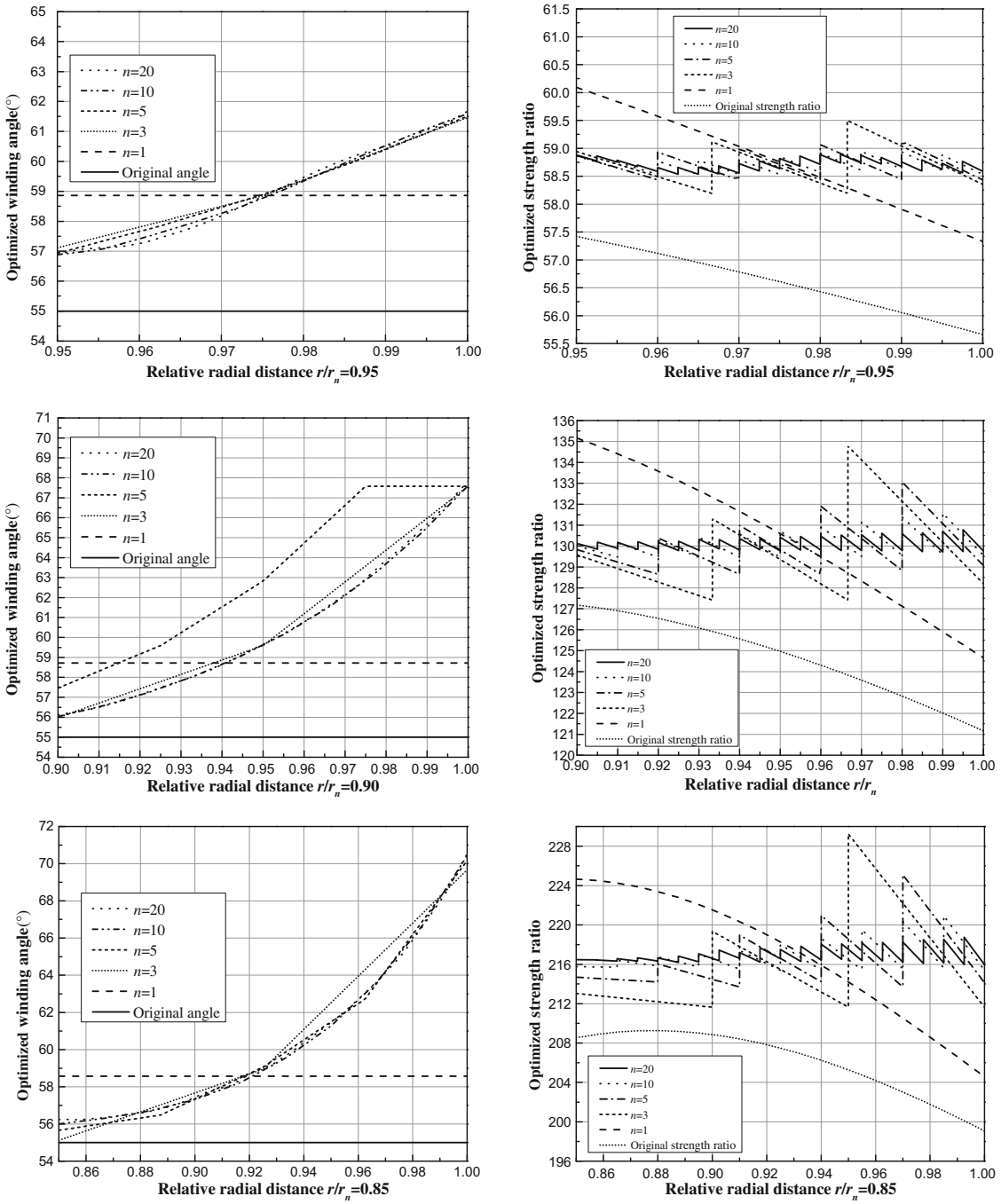

Fig. 4 The optimized winding angle and the corresponding strength ratio distributions via thickness of E-glass/epoxy

The optimized winding angle sequence, the maximum strength ratio and the strength ratio distribution via thickness are calculated, respectively.

4.1 T300/934 cylinders

For T300/934 cylinders, the optimized winding angle sequence for different layer number n and the corresponding strength ratio distributions via thickness are shown in Fig. 3 for $r_0/r_n = 0.95, 0.90, 0.85, 0.80, 0.75, 0.70$ and 0.65.

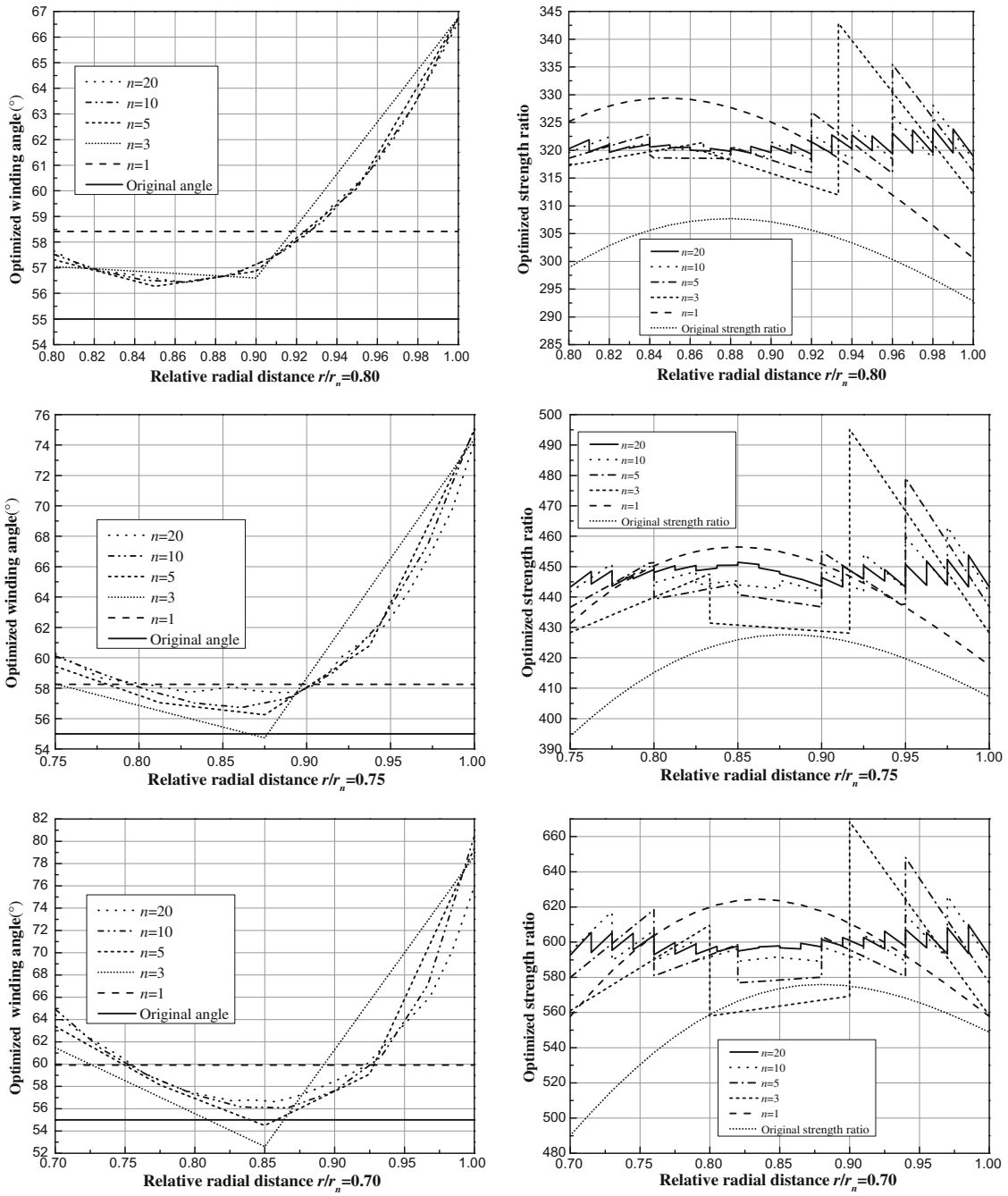

Fig. 4 continued

From the figures we find that, for single-layered cylinder, the winding angles distribute in range 54°–57° for $r_0/r_n = 0.95 - 0.65$. This conclusion is consistent with the paper [24].

For a multi-layered thin-walled FW cylinder, such as $r_0/r_n = 0.95$, the optimized winding angle, which is stable and smooth for large number of n, increases versus thickness outward, whose minimum and maximum appear on the inner and outer surface, respectively. With the increase number of n, the maximum strength ratio and more uniform strength distribution are achieved. With thicker wall thickness, such as $r_0/r_n = 0.80$, the optimized winding angle increases rapidly near the inner surface and the optimized winding angle decreases rapidly near the outer surface, like a parabola. For large number of n, the maximum strength ratio and more

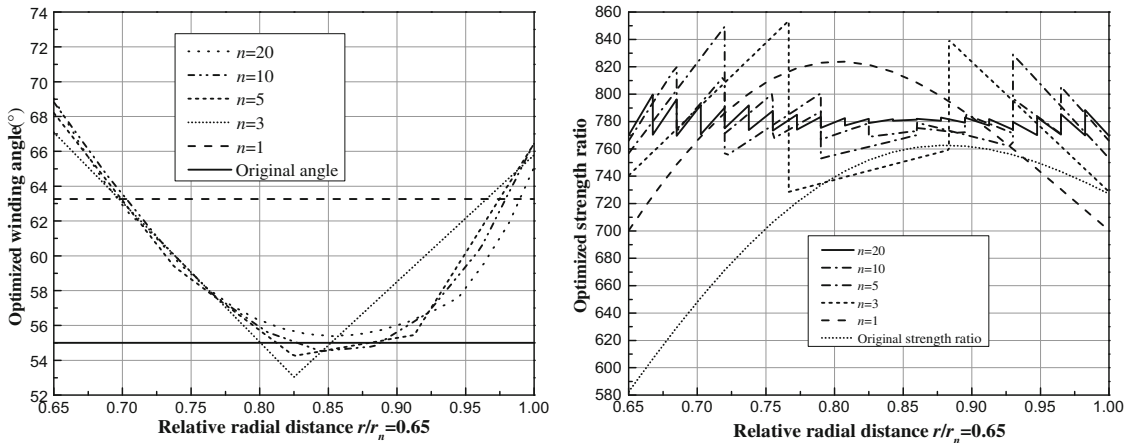

Fig. 4 continued

Table 6 The strength ratio in 20-layer cylinder of original and optimized winding angle of (b) E-glass/epoxy

r_0/r_n	Original winding angle				Optimized winding angle			
	Maximum	Minimum	D-value	Performance (%)	Maximum	Minimum	D-value	Performance (%)
0.95	57.421	55.665	1.76	3.06	58.894	58.537	0.357	0.61
0.90	127.180	121.161	6.02	4.73	130.783	129.716	1.066	0.82
0.85	209.269	199.061	10.21	4.88	218.746	215.965	2.781	1.27
0.80	307.677	292.823	14.85	4.83	323.977	318.945	5.033	1.55
0.75	427.566	394.203	33.36	7.80	453.787	443.286	10.501	2.31
0.70	575.960	490.068	85.89	14.91	609.855	592.580	17.275	2.83
0.65	762.576	582.509	180.07	23.61	799.652	769.562	30.090	3.76

uniform strength distribution are achieved. For very thick cylinders, such as $r_0/r_n = 0.65$, the optimized winding angle reaches nearly 90° near the inner surface and uniform strength distribution cannot be achieved. Obviously, it is difficult to achieve uniform strength ratio via thickness only by changing winding angle. A 20-layer strength ratio variation is compared in Table 5.

From the results, for original scheme, the difference of strength ratio via thickness for $r_0/r_n = 0.95 - 0.65$ is 14.18, 15.16, 14.70, 25.61, 39.12, 51.34, 61.90 %, respectively, while that of the optimized scheme is 1.17, 2.88, 6.06, 17.98, 30.07, 41.22, 51.29 %, respectively. The optimized scheme leads to more uniform strength ratio than the original one, and the minimum strength is much higher than that of the original scheme.

4.2 E-glass/epoxy cylinders

For E-glass/epoxy cylinders, the optimized winding angle sequence for different layer number n and the corresponding maximum strength ratio are shown in Fig. 4.

The general trends of winding angle of E-glass/epoxy cylinders are the same with that of T300/934 cylinders. It is worth to emphasize that the variation of the optimized winding angle is stable and smooth for large number n, and with the increase number of n, the maximum strength ratio and more uniform strength distribution via thickness can be achieved easily. It suggests that the material property has great influence on strength ratio distribution via thickness. The more difference elasticity coefficients in different directions, the more difficult to achieve an optimal winding angle scheme and large difference distribution in strength ratio via thickness are produced.

The strength ratio variation in 20-layer cylinder is shown in Table 6. From the results, for original scheme, the difference of strength ratio via thickness for $r_0/r_n = 0.95 - 0.65$ is 3.06, 4.73, 4.88, 4.83, 7.80, 14.91, 23.61 %, respectively, while the optimized scheme is 0.61, 0.82, 1.27, 1.55, 2.31, 2.83, 3.76 %, respectively. More uniform strength ratio distribution is achieved, and their minimum strength ratio is improved significantly.

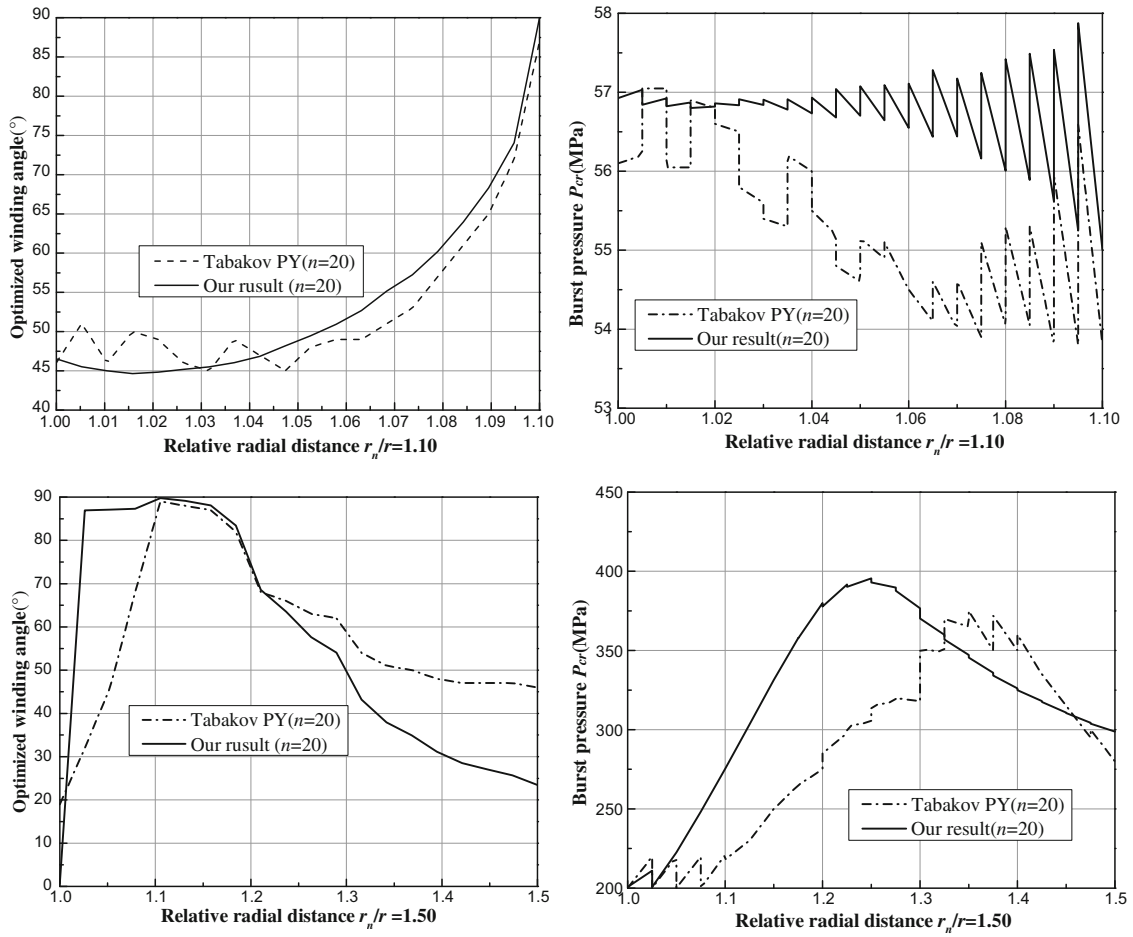

Fig. 5 The optimized winding angle and the corresponding strength ratio distributions via thickness of T300/5208

4.3 Comparison of multi-angle winding vessel of T300

In order to prove the accuracy of the results in this paper, here the 20-layered filament-wound cylinder in [24] is chosen and compared for strength ratio $R = 1$, $r_n/r_0 = 1.1, 1.5$.

The optimized winding angle sequence and distribution of the burst pressures via the thickness of a 20-layered cylinder are shown in Fig 5. From the results, for the thin-walled FW cylinder ($r_n/r = 1.1$), it is found that the two optimized winding angle sequences are very similar, and the distribution of the burst pressures of this paper is much better than those of [24]. For very thick cylinders ($r_n/r = 1.5$), it is found that there is no difference between the distribution of the burst pressures.

5 Conclusion

The investigation leads to conclusions:

(1) A suitable optimization method has great influence to the optimized winding angle sequence. Numeric results show that the combined complex–steepest descent method has better efficiency to achieve the optimization solution.
(2) The material property has great influence on strength ratio distribution via thickness. Large difference in elasticity coefficients in different directions, more evident variation winding angle should be adopted to achieve more uniform strength ratio, so the corresponding strength ratio distributions of E-glass/epoxy are much better than T300/934.

(3) The material utilization and working pressure can be increased by proper winding angle variation, and several optimization winding angle sequence schemes are found for different radius ratio cylindrical vessels made of E-glass/epoxy or T300/934.
(4) In this paper, more accurate calculation results are given for multi-layered thin-walled FW cylinder. It is difficult to achieve uniform strength ratio via thickness for carbon fiber cylinder by changing winding angle, and the strength ratios of the carbon fibers are approximately double the values of the glass fibers. Therefore, the carbon fiber is not suitable for a thick-walled FW cylinder.

References

1. Tsai, S.W.: Composite design. In: Think Composites, 4th edn. Dayton (1988)
2. Skinner, M.L.: Trends, advances and innovations in filament winding. Reinf. Plast. **2**, 28–33 (2006)
3. Mertiny, P., Ellyin, F., Hothan, A.: An experimental investigation on the effect of multi-angle filament winding on the strength of tubular composite structures. Compos. Sci. Technol. **64**, 1–9 (2004)
4. Soden, P.D., Kitching, R., Tse, P.C., Tsavalas, Y., Hinton, M.J.: Influence of winding angle on the strength and deformation of filament-wound composite tubes subjected to uniaxial and biaxial loads. Compos. Sci. Technol. **46**, 363–378 (1993)
5. Soden, P.D., Leadbetter, D., Griggs, P.R., Eckold, G.C.: The strength of a filament wound composite under biaxial loading. Composites **9**, 247–250 (1978)
6. Spencer, B., Hull, D.: Effect of winding angle on the failure of filament wound pipe. Composites **9**, 263–271 (1978)
7. Soden, P.D., Kitching, R., Tse, T.C.: Experimental failure stresses for ±55 filament wound glass fiber reinforced plastic tubes under biaxial loads. Composites **20**, 125–135 (1989)
8. Ellyin, F., Carroll, M., Kujawski, D., Chiu, A.S.: The behavior of multidirectional filament wound fiber glass/epoxy tubulars under biaxial loading. Composites **28A**, 781–790 (1997)
9. Antoniou, A.E., Kensche, C., Philippidis, T.P.: Mechanical behavior of glass/epoxy tubes under combined static loading. Part I: experimental. Compos. Sci. Technol. **69**, 2241–2247 (2009)
10. Cohen, D.: Influence of filament winding parameters on composite vessel quality and strength. Compos. Part A Appl. Sci. Manuf. **28**, 1035–1047 (1997)
11. Mertiny, P., Ellyin, F., Hothan, A.: Stacking sequence effect of multi-angle filament wound tubular composite structures. J. Compos. Mater. **38**, 1095–1113 (2004)
12. Roy, A.K., Tsai, S.W.: Design of thick composite cylinders. J. Press. Vessel Technol. **110**, 255–262 (1988)
13. Xing, J.Z., Geng, P., Yang, T.: Stress and deformation of hybrid filament-wound thick cylinder vessel under internal and external pressure. Compos. Struct. **131**, 868–877 (2015)
14. Kim, J.S., Kim, C.G., Hong, C.S.: Optimum design of composite structures with ply drop using genetic algorithm and expert system shell. Compos. Struct. **46**, 171–187 (1999)
15. Farshi, B., Rabiei, R.: Optimum design of composite laminates for frequency constraints. Compos. Struct. **01**, 587–597 (2007)
16. Naik, G.N., Gopalakrishnan, S., Ganguli, R.: Design optimization of composites using genetic algorithms and failure mechanism based failure criterion. Compos. Struct. **83**, 354–367 (2008)
17. Paluch, B., Grédiac, M., Faye, A.: Combining a finite element programme and a genetic algorithm to optimize composite structures. Compos. Struct. **83**, 284–294 (2008)
18. Park, C.H., Saouab, A., Breard, J., et al.: An integrated optimization for the weight, the structural performance and the cost. Compos. Sci. Technol. **69**, 1101–1107 (2009)
19. Irisarri, F.X., Bassir, D.H., Carrere, N., et al.: Multiobjective stacking sequence optimization for laminated composite structures. Compos. Sci. Technol. **69**, 983–990 (2009)
20. Almeida, F.S., Awruch, A.M.: Design optimization of composite laminated structures using genetic algorithms and finite element analysis. Compos. Struct. **88**, 443–454 (2009)
21. Apalak, M.K., Yildirim, M., Ekici, R.: Layer optimization for maximum fundamental frequency of laminated composite plates. Compos. Sci. Technol. **68**, 537–550 (2008)
22. Todoroki, A., Sekishiro, M.: New iteration fractal branch and bound method for stacking sequence optimizations of multiple laminates. Compos. Struct. **81**, 419–426 (2007)
23. Grédiac, M.: On the stiffness design of thin woven composites. Compos. Struct. **51**, 245–255 (2001)
24. Tabakov, P.Y., Summers, E.B.: Lay-up optimization of multilayered anisotropic cylinders based on a 3-D elasticity solution. Compos. Struct. **84**, 374–384 (2006)
25. Liu, K.S., S W, Tsai: A progressive quadratic failure criterion for a laminate. Compos. Sci. Technol. **58**, 1023–1032 (1998)
26. Rao, S.S.: Engineering Optimization Theory and Practice. Wiley, Hoboken (2009)
27. Goetschel, D.B., Radford, D.W.: Analytical development of through-thickness properties of composite laminates. J. Adv. Mater. **29**, 37–46 (1997)